NUCLEAR SCIENCE AND TECHNIQUES **26**, 030101 (2015)

Small angle X-ray scattering beamline at SSRF*

TIAN Feng (田丰), LI Xiu-Hong (李秀宏), WANG Yu-Zhu (王玉柱), YANG Chun-Ming (杨春明), ZHOU Ping (周平), LIN Jin-You (林金友), ZENG Jian-Rong (曾建荣), HONG Chun-Xia (洪春霞), HUA Wen-Qiang (滑文强), LI Xiao-Yun (李小芸), MIAO Xia-Ran (缪夏然), BIAN Feng-Gang (边风刚),† and WANG Jie (王劼)

Shanghai Institute of Applied Physics, Chinese Academy of Sciences, Shanghai 201204, China

(Received September 30, 2014; accepted in revised form April 9, 2015; published online June 20, 2015)

Beamline BL16B1 at Shanghai Synchrotron Radiation Facility (SSRF) is dedicated to studying the microstructure and dynamic processes of polymers, nanomaterials, mesoporous materials, colloids, liquid crystals, metal materials, etc. At present, SAXS, wide angle X-ray scattering (WAXS), simultaneous SAXS/WAXS, grazing incident SAXS, and anomalous SAXS techniques are available for end user to conduct diverse experiments at this beamline. The sample-to-detector distance is adjustable from 0.2 m to 5 m. The practicable $\boldsymbol{q}$-range is 0.03–3.6 nm^{-1} at incident X-ray of 10 keV for conventional SAXS whilst a continuous $\boldsymbol{q}$-region of 0.06–33 nm^{-1} can be achieved in simultaneous SAXS/WAXS mode. Time-resolved SAXS measurements in sub-second level was achieved by the beamline upgrating in 2013. This paper gives detailed descriptions about the status, performance and applications of the SAXS beamline.

Keywords: Small angle X-ray scattering (SAXS), Wide angle X-ray scattering, Grazing incident SAXS, Anomalous SAXS

DOI: 10.13538/j.1001-8042/nst.26.030101

I. INTRODUCTION

As one of the third-generation synchrotron radiation light source, Shanghai Synchrotron Radiation Facility (SSRF) [1] is now operated in a top-up injection mode with a constant electron beam current of 240 mA. The small angle X-ray scattering (SAXS) beamline (BL16B1) is one of the seven Phase-I beamlines of SSRF, designed for measurements of small angle X-ray scattering (SAXS), wide angle X-ray scattering (WAXS), anomalous small angle X-ray scattering (ASAXS), and grazing incident small angle X-ray scattering (GISAXS) of appropriate samples. Constructed and opened to users in 2009, and upgraded in 2013, the beamline enables time-resolved studies on structural transitions in the sub-second level. Most users' experiments performed on this beamline refer to kinetics, dynamics and rheology on materials with nanoscale structures, such as polymers, nanomaterials, mesoporous materials, colloids, liquid crystals, metal materials, etc. In this paper, we present a detail description about the SAXS beamline and station.

II. BEAMLINE CONFIGURATION AND TECHNIQUE SPECIFICATIONS

The photon source of bending magnet of SSRF delivers X-rays of 5 keV to 20 keV. The beam with 1.2×0.12 $mrad^2$ divergence can be accepted by the optics system. The beamline optics consists of a Si(111) flat double crystal monochromator (DCM) and a double focusing toroidal mirror. Optical layout of the beamline is shown in Fig. 1. Generally, the beamline works at 10 keV (0.124 nm) for user experiments.

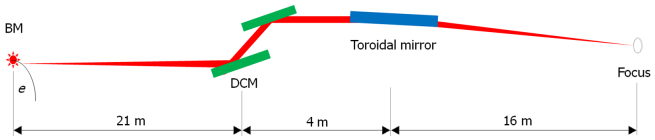

Fig. 1. (Color online) Optical layout of SAXS beamline at SSRF.

Specifications of the SAXS beamline are as follows:

Energy range: 5–20 keV;

Energy resolution: 4.0×10^{-4}@10 keV;

Flux: $\sim 3 \times 10^{11}$ phs/s@10 keV and 240 mA;

Focus size: $\sim$ 0.4 mm (H)×0.5 mm (V).

The results of spot size and rocking curve measured on BL16B1 are shown in Fig. 2.

The endstation of BL16B1 is shown in Fig. 3. The detectors are Mar165 CCD for SAXS, and INEL CPS120 (a one-dimensional arc gas detector) for WAXS. The beam intensity monitor before sample is a N_2 gas ionization chamber, and the monitor after sample adsorption is a photodiode in the beam stop. Two scatter-less slits (Xenocs) are used to depress parasitic scattering. The sample holder is mounted onto an optical table. The distance of sample to SAXS detector can be adjusted up to 5 m, scattering from a sample transmits in vacuum, passing Kapton window to hit the detector. There are sample stages for SAXS, GISAXS or WAXS (2D). The $\boldsymbol{q}$ ranges are 0.03–3.6 nm^{-1} for SAXS measurement and 4.5–33 nm^{-1} for WAXS measurement at 10 keV. And a continuous $\boldsymbol{q}$ range of 0.06–33 nm^{-1} can be obtained in simultaneous SAXS/WAXS. Two conventional modes in sample-to-director distance of 2 m and 5 m have been provided to users, and the $\boldsymbol{q}$ ranges are 0.08–3.6 nm^{-1} at 2 m, and 0.03–1.4 nm^{-1} at 5 m.

* Supported by the National Basic Research Program of China (Nos. 2011CB911104, 2011CB606104, and 2011CB605604), National Natural Science Foundation of China (Nos. 11305249, 11005143, 50903089, 51273210, 11405259, 51303200, and 11305242), and Knowledge Innovation Program of Chinese Academy of Sciences

† Corresponding author, bianfenggang@sinap.ac.cn

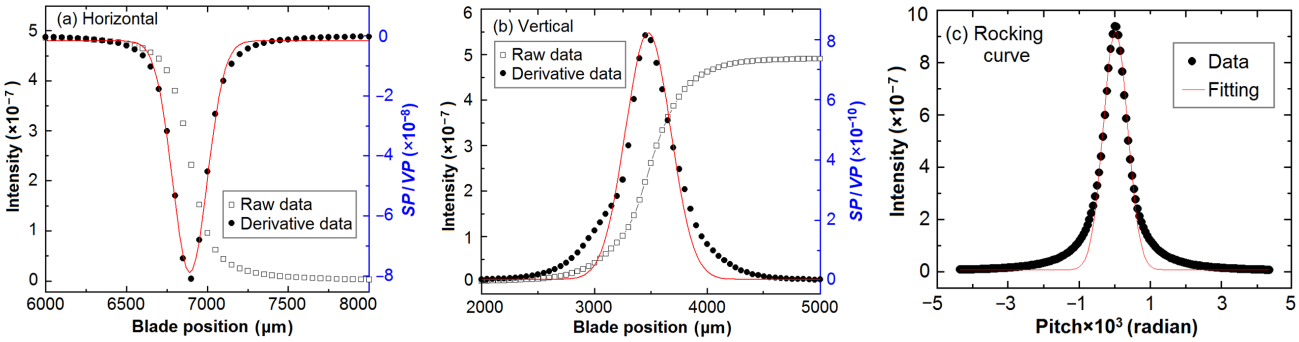

Fig. 2. (Color online) Results of spot size measurement of BL16B1.

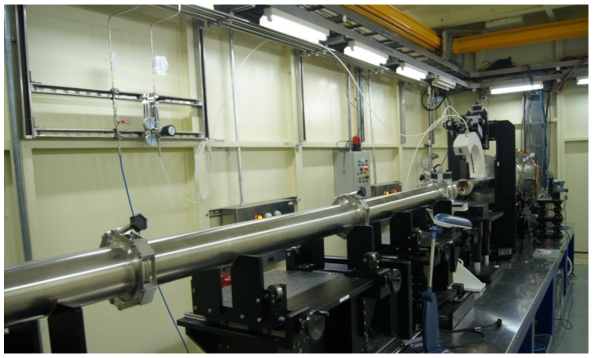

Fig. 3. (Color online) Endstation of BL16B1.

The beamline control system is based on an EPICS platform in Linux operation system, which is convenient to communicate among the devices. The CPS 120 detector works currently on a Labview platform in Windows operation system, it will be integrated into EPICS in future. Besides the foreseen sample surroundings, the users have the possibility to install their own specialized sample devices [2–5]. Technical boundary conditions, user friendliness and reliability have been considered as important criteria.

III. METHODOLOGY

Techniques of the beamline include SAXS, WAXS, simultaneous SAXS/WAXS, GISAXS and ASAXS.

A. SAXS technique

SAXS in transmission mode can be used for studying materials, such as polymer, nanomaterials, metal, bio-materials, etc. [6–10]. Most of the SAXS experiments finished are *in-situ* studies on microstructure evolution of different samples, such as *in-situ* stretching of polymers and fiber at different temperatures. A typical work [11] is described as follows.

The long time evolution of extension-induced crystallization of polyethylene oxide (PEO) was investigated by a combination of rheological measurement and *in-situ* SAXS, aimed at understanding dynamic changes in spatial arrangement of nuclei, in terms of both the chain stretching and orientation. The structural evolution in the small strain region is shown in Fig. 4.

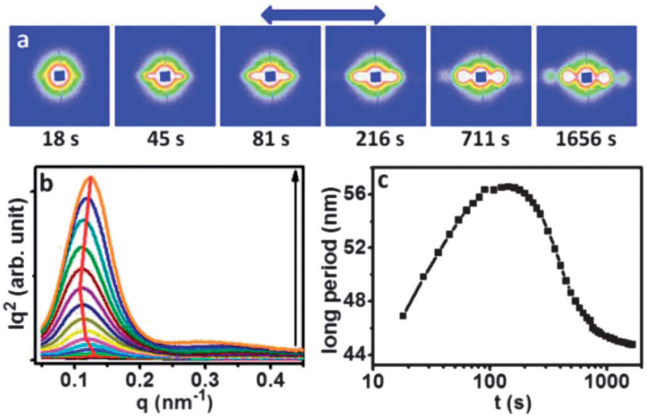

Fig. 4. (Color online) Results of *in-situ* SAXS measurements of a polyethylene oxide sample (a) time evolution of the 2D SAXS pattern with a strain rate of $25\,s^{-1}$, (b) the 1D intensity profiles, (c) evolution of the long period crystallization.

B. Simultaneous SAXS/WAXS measurement

Figure 5(a) shows instrumentation sketch of the simultaneous SAXS/WAXS measurement. In order to obtain a continuous scattering vector $\boldsymbol{q}$ across the SAXS and WAXS collectable regions, the simultaneous SAXS/WAXS technique was developed, with the determinable range of SAXS measurement being $\boldsymbol{q} = 0.06$–$3.50\,nm^{-1}$, while that of WAXS being $\boldsymbol{q} = 2.50$–$34.8\,nm^{-1}$. Therefore, a continuous $\boldsymbol{q}$ can be obtained with a continuous $\boldsymbol{q}$ range of 0.06–$33\,nm^{-1}$ (Fig. 5(b)). Simultaneous SAXS/WAXS is important for studying fiber stretching, liquid crystal and self-assembly system [12, 13].

The hardware is shown schematically in Fig. 6. The Mar165 CCD is the SAXS detector, and the 1D arc PSD (CPS 120) is the WAXS detector. The SAXS detector has a trig-

ger signal to control other equipments to work synchronously. The shutter, WAXS and SAXS detectors, can work synchronously through a pulse generator. Experimental results of simultaneous SAXS/WAXS for silver Behenate performed on BL16B1 are shown in Fig. 5(b). The data of SAXS and WAXS are combined through scaling the SAXS data with a factor to equal their integral area in the overlap region.

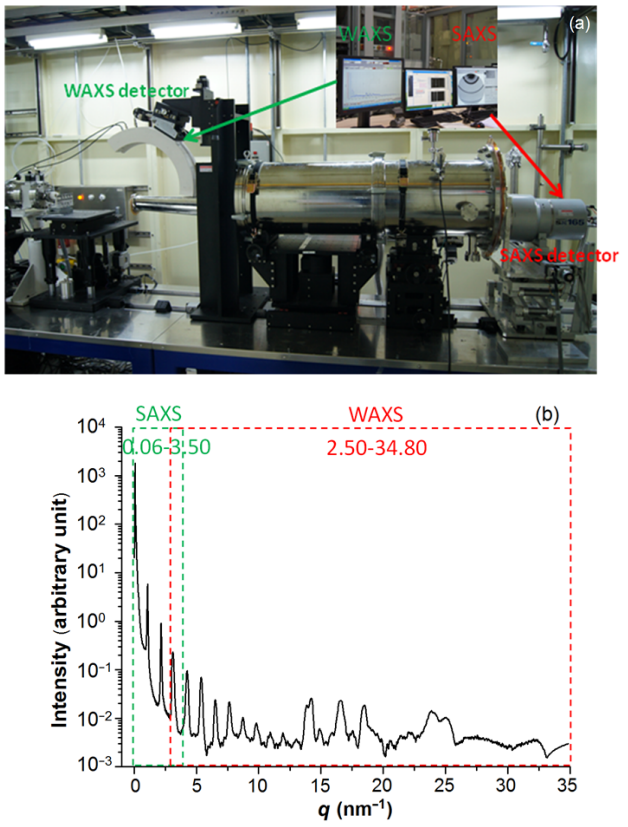

Fig. 5. (Color online) The SAXS/WAXS experiment station at BL16B1beamline (a) and the SAXS/WAXS measurements for silver behenate (b).

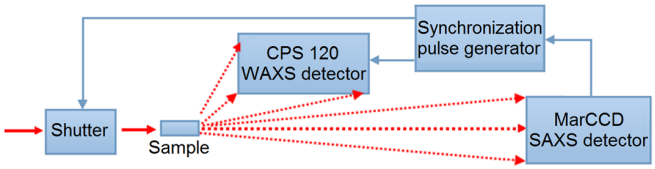

Fig. 6. (Color online) Hardware schematics of the simultaneous SAXS/WAXS technique.

C. Grazing incidence SAXS

GISAXS is a powerful tool for studying film surface and interface structures [14–17]. A Kohzu tilt stage is used as GISAXS sample stage (Fig. 7). The incidence angle of X-rays can be adjusted by the sample stage within an accuracy of $0.001°$. In principle, the size of samples should be larger than $0.5\,\mathrm{cm}$ $(w) \times 1\,\mathrm{cm}$ (l).

The GISAXS experiments [18–21] performed on BL16B1

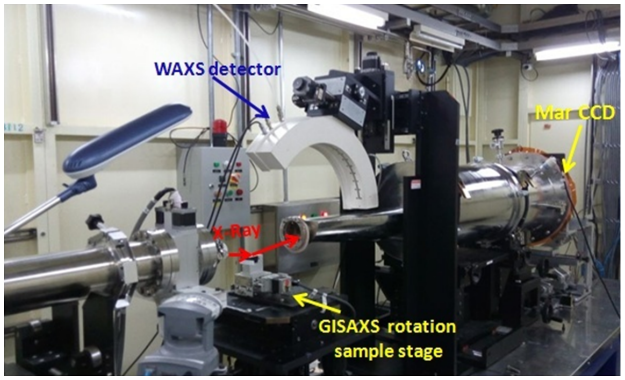

Fig. 7. (Color online) The GISAXS setup at BL16B1.

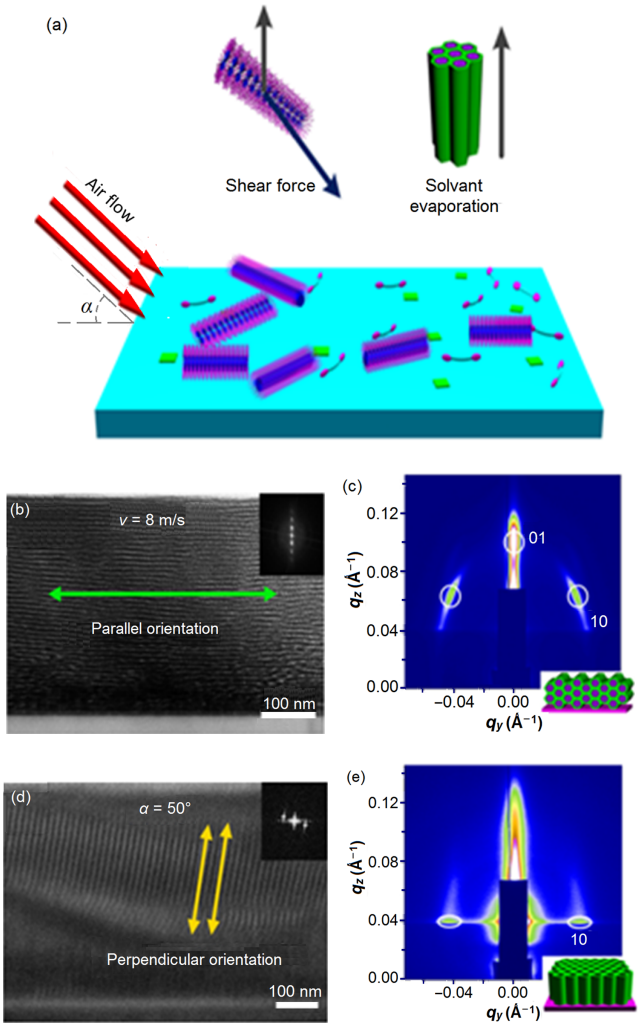

Fig. 8. (Color online) Schematic of air flow induced orientation control of titania mesochannels (a); the results of parallel alignment: (b), TEM, (c), GISAXS; and the results of vertical alignment: (d), TEM, (e), GISAXS.

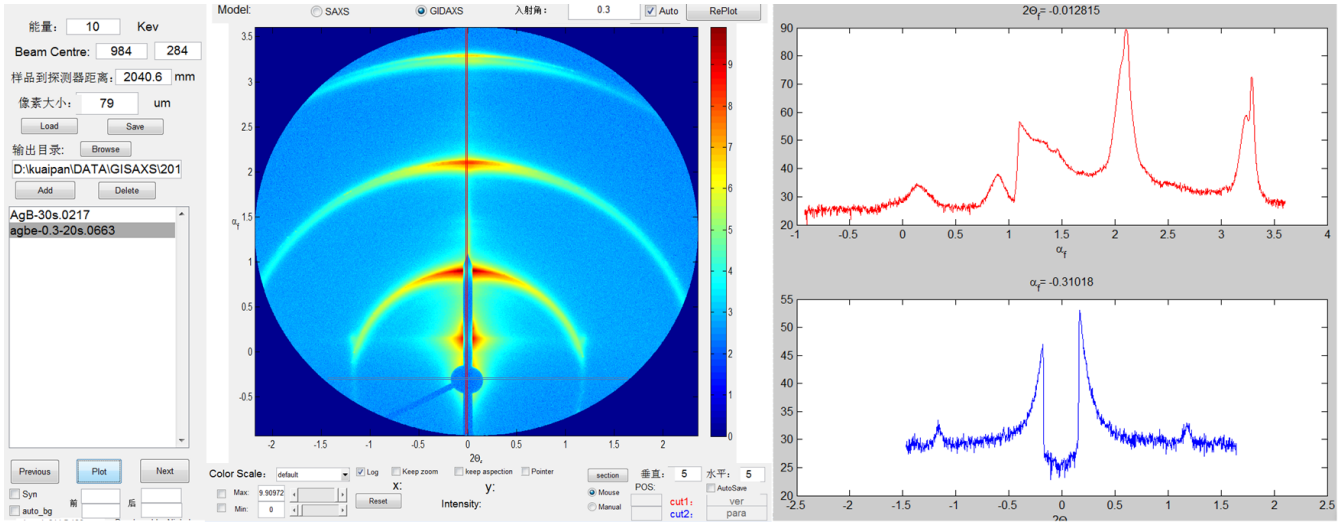

Fig. 9. (Color online) Interfaces of "Pre-GISAXS".

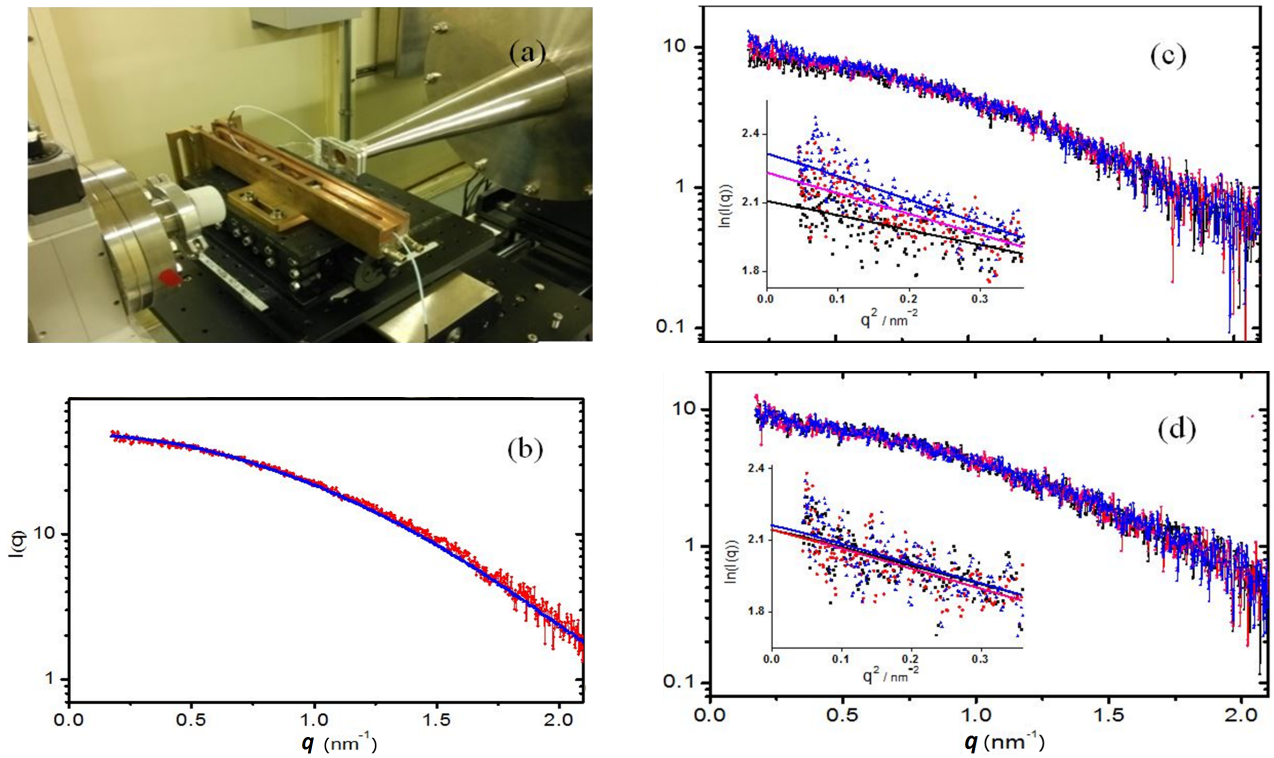

Fig. 10. (Color online) Peristaltic device for bio-solution SAXS measurement (a); solution scattering profiles of lysozyme using peristaltic-collection mode (red) and the standard curve (blue) (b); SAXS profiles of lysozyme using stationary-collection mode (c) and peristaltic-collection mode (d) in the exposure order of black, red and blue, 100 s each. Inserts show the Guinier plot of two modes.

include the finding of a novel orientation of mesochannels in mesostructured thin films, results were published in [22].

As shown in Fig. 8(a), uniaxially oriented mesoporous titania films in any uniaxial alignment direction were prepared by manipulating the magnitude and incidence angle of a shear-force of a hot air-flow. According to the TEM and GISAXS results of Figs. 8(b)–8(e), orientation of the mesochannels can be well controlled into parallel, vertical or oblique, with any angle with respect to the plane, by simply regulating the rate and incident angle of the air flow.

A one dimension profile along the vertical and horizontal directions can be obtained from a two dimension GISAXS pattern using "Pre-GISAXS" (Fig. 9) [23].

D. Anomalous SAXS

Depending on energy tunability, ASAXS can be conducted. ASAXS of aluminum alloys (7150 and 7085 Al alloy) have been carried out. The SAXS patterns of 7150 Al alloy were obtained at various energies below the Zn K-edge. It was found that the scattering intensity increased obviously with decreasing energy. Due to absorption, thickness of the alloy sample should be less than 150 μm.

E. SAXS study of protein solution

To reduce radiation damage, we have developed a peristaltic device with thermo controller for solution SAXS measurements (Fig. 10(a)) [24]. Figures 10(b)–10(c) show the scattering data of lysozyme collected at BL16B1 using this device, indicating that the device is able to reduce the radiation damage for biomacromolecule solution samples.

F. Supporting conditions and data processing

The BL16B1 beamline at SSRF offers support for end users to carry out experimental research. Samples can be prepared in the support laboratories with ultra-pure water system, magnetic stirrer, electronic balance, ultrasonic apparatus, centrifuge, electric oven, vacuum drying apparatus, polarizing microscope and AFM. And some *in-situ* devices are available, such as Linkam THMS600 heating stage (−196 °C to 600 °C), Linkam CSS450 shearing system (ambient to 450 °C), Linkam TS1500 heating stage (ambient to 1500 °C), *in-situ* fiber stretching (maximum tension: 1000 N) device (ambient to 500 °C), and helium-atmosphere sample chamber to protect the samples from oxidation.

A few widely-used packages of data processing have been developed, such as Irena, Nika, X-polar, FIT2D, etc. Special data process services such as remote data access and data archive [25] are also available on request.

IV. CONCLUSION

The SAXS beamline at SSRF provides a powerful support for studying microstructure of polymers, fibers and nanostructure/mesoporous materials. The techniques available in the beamline include SAXS, WAXS, ASAXS, GISAXS, and time-resolved simultaneous SAXS/WAXS on structural transitions in the sub-second time region and partly ordered systems with a scaling of 1 nm to 240 nm in real-space. More techniques will be developed at BL16B1, such as USAXS technique based on Bonse-Hart camera system and microfocus SAXS. Still more common *in-situ* devices to facilitate the users will be developed. A complete SAXS data analysis platform will be established for data pretreatment, SAXS and WAXS data analysis, etc.

[1] Xu H J and Zhao Z T. Current status and progresses of SSRF project. Nucl Sci Tech, 2008, **19**: 1–6. DOI: 10.1016/S1001-8042(08)60013-5

[2] Liu G M, Zheng L C, Zhang X Q, *et al*. Critical stress for crystal transition in poly(butylene succinate)-based crystalline–amorphous multiblock copolymers. Macromolecules, 2014, **47**: 7533–7539. DOI: 10.1021/ma501832z

[3] Li F G, Zhang J, Dai Y B, *et al*. Study of the influence of TiB_2 particles on the melt structure of the hypoeutectic Al–Cu alloy by small angle X-ray scattering. Mater Chem Phys, 2014, **143**: 471–475. DOI: 10.1016/j.matchemphys.2013.10.027

[4] Wei Z Z, Lin J Y, Tian F, *et al*. Synchronous stimuli of biodegradable poly(butylene succinate-co-terephthalate) copolymer via uniaxial stretching at varying temperatures. J Polym Sci Pol Phys, 2014, **9**: 640–649. DOI: 10.1002/polb.23681

[5] Huang Y F, Xu J Z, Xu J Y, *et al*. Self-reinforced polyethylene blend for artificial joint application. J Mater Chem B, 2014, **2**: 971–980. DOI: 10.1039/C3TB21231A

[6] Pan H, Zhang Y P, Shao H L, *et al*. Nanoconfined crystallites toughen artificial silk. J Mater Chem B, 2014, **2**: 1408–1414. DOI: 10.1039/C3TB21148G

[7] Shen J L, Xu L F, Wang C P, *et al*. Dynamic and quantitative control of the DNA-mediated growth of gold plasmonic nanostructures. Angew Chem Int Edit, 2014, **32**: 8338–8342. DOI: 10.1002/anie.201402937

[8] Liu D M, Xiong B Q, Bian F G, *et al*. In situ studies of microstructure evolution and properties of an Al–7.5Zn–1.7Mg–1.4Cu–0.12Zr alloy during retrogression and reaging. Mater Design, 2014, **56**: 1020–1024. DOI: 10.1016/j.matdes.2013.12.006

[9] Su H Y, Liu Y H, Wang D, *et al*. Amphiphilic starlike dextran wrapped superparamagnetic iron oxide nanoparticleclsuters as effective magnetic resonance imaging probes. Biomaterials, 2013, **34**: 1193–1203. DOI: 10.1016/j.biomaterials.2012.10.056

[10] Liu F, Prehm M, Zeng X B, *et al*. Skeletal cubic, lamellar, and ribbon phases of bundled thermotropic bolapolyphiles. J Am Chem Soc, 2014, **136**: 6846–6849. DOI: 10.1021/ja502410e

[11] Tian N, Liu D, Li X Y, *et al*. Relaxation propelled long period change in the extension induced crystallization of polyethylene oxide. Soft Matter, 2013, **9**: 10759–10767. DOI: 10.1039/C3SM52152D

[12] Leonard M J and Strey H H. Phase diagrams of stoichiometric polyelectrolyte–surfactant complexes. Macromolecules, 2003, **36**: 9549–9558. DOI: 10.1021/ma034352c

[13] Shi Z H, Cheng D Z, Lu H J, *et al*. Self-assembled hierarchical structure evolution of azobenzene-containing linear-dendritic liquid crystalline block copolymers. Soft Matter, 2012, **8**: 6174–6184. DOI: 10.1039/C2SM07249A

[14] Zhang J Q, Posselt D, Smilgies DM, *et al*. Lamellar diblock copolymer thin films during solvent vapor annealing studied by GISAXS: different behavior of parallel and perpendicular lamellae. 2014, **47**: 5711–5718. DOI: 10.1021/ma500633b

[15] Huang Y C, Tsao C S, Chuang C M, *et al*. Small- and wide-angle X-ray scattering characterization of bulk heterojunction

polymer solar cells with different fullerene derivatives. J Phys Chem C, 2012, **116**: 10238–10244. DOI: 10.1021/jp210140j

[16] Ahn B, Hirai T, Jin S, *et al*. Hierarchical structure in nanoscale thin films of a poly(styrene-*b*-methacrylate grafted with POSS) (PS_{214}-*b*-$PMAPOSS_{27}$). Macromolecules, 2010, **43**: 10568–10581. DOI: 10.1021/ma101276d

[17] Liang Y Y, Feng D Q, Guo J C, *et al*. Regioregular oligomer and polymer containing thieno[3,4-*b*]thiophene moiety for efficient organic solar cells. Macromolecules, 2009, **42**: 1091–1098. DOI: 10.1021/ma8023969

[18] Dou J H, Zheng Y Q , Lei T, *et al*. Systematic investigation of side-chain branching position effect on electron carrier mobility in conjugated polymers. Adv Funct Mater, 2014, **40**: 6270–6278. DOI: 10.1002/adfm.201401822

[19] Shan F, Lu X M, Guan J F, *et al*. Airflow-field-induced sandwich-type membrane of block copolymer for selective ion separation. Macromol Rapid Comm, 2014, **35**: 735–740. DOI: 10.1002/marc.201300880

[20] Sun J H, Zhang Q H, Ding R M, *et al*. Contamination-resistant silica antireflective coating with closed ordered mesopores. Phys Chem Chem Phys, 2014, **16**: 16684–16693. DOI: 10.1039/c4cp01032a

[21] He Q Y, Dai H, Tan X P, *et al*. Synthesis and characterization of room temperature columnar mesogens of cyclotriphosphazene with Schiff base units. J Mater Chem C, 2013, **1**: 7148–7154. DOI: 10.1039/C3TC31371A

[22] Shan F, Lu X M, Zhang Q, *et al*. A facile approach for controlling the orientation of one-dimensional mesochannels in mesoporous titania films. J Am Chem Soc, 2012, **134**: 20238–20241. DOI: 10.1021/ja309168f

[23] Zhao N, Bian F G, Wang Y Z, *et al*. Calibrating scattering angle in wide angle X-ray scattering experiment. Sci China Ser G-Phys Mech Astron, 2015, **45**: 017001. (in Chinese) DOI: 10.1360/SSPMA2014-00106

[24] The resource for macromolecular SAXS. http://www.bioisis.net/tutorial

[25] HU Z, MI Q, ZHENG L, *et al*. EPICS data archiever at SSRF beamlines. Nucl Sci Tech, 2014, **25**: 020103. DOI: 10.13538/j.1001-8042/nst.25.020103